The influence of zeolite morphology on the conversion of methane to methanol on copper-exchanged omega zeolite (MAZ)

Catalysis Science & Technology

PAPER

View Article Online
View Journal | View Issue

Cite this: *Catal. Sci. Technol.*, 2019, **9**, 2806

The influence of zeolite morphology on the conversion of methane to methanol on copper-exchanged omega zeolite (MAZ)†

Amy J. Knorpp,[a] Mark A. Newton,[a] Vitaly L. Sushkevich,[b] Patrik P. Zimmermann,[b] Ana B. Pinar*[b] and Jeroen A. van Bokhoven*[ab]

Received 3rd January 2019,
Accepted 17th April 2019

DOI: 10.1039/c9cy00013e

rsc.li/catalysis

Methane is often flared due to the heavy economic burden of transportation, particularly at rural petroleum extraction sites. Directly converting methane to methanol is possible through a stepwise process with copper-exchanged zeolites. Factors affecting this conversion are not yet fully understood. Omega zeolite (MAZ) can yield 197 μmol per gram-zeolite, the highest reported thus far. Here we show that the synthesis and resulting morphology of the zeolite play an enormous role in the yield of methanol. High yields are only achieved when the zeolite has a longer stick-like bundled morphology (2–4 μm by 100 nm). When the zeolite forms small spherulitic aggregates, the methanol yield is severely diminished (60–97 μmol-methanol per gram-zeolite). This difference originates from minute changes in the synthesis procedure, emphasizing the extreme sensitivity of zeolite properties towards synthesis conditions. This work shows that selecting a parent zeolite is crucial and is an opportunity for process optimization to achieve high and industrially-relevant methanol yields.

Introduction

The market price of methane doesn't always meet the costs of its compression and transportation. This is particularly true at distant crude oil production facilities where methane can accompany more desired products like crude oil. The fate of this methane is determined by local environmental regulations and local economics of transportation. In the end, this leads to large amounts of methane being wasted through combustion (flaring).[1–3] This process, though wasteful, is better for the environment than direct emissions of methane to the atmosphere, since carbon dioxide has a lower greenhouse gas effect than methane. Alternatively, methane can be converted to other chemicals that are more cost effective due to easier transportation or higher market value.[4] Such conversions are fundamentally challenging as desired products can be highly reactive, and the conditions for activating a carbon–hydrogen bond in methane can also result in overoxidation (*i.e.* formation of CO_2) of the products.[5]

Converting methane to methanol is one such process that has garnered attention academically and industrially.[6–9] Methane can be converted to methanol by an energy-intensive two-step process that first requires steam reforming and then catalytic conversion of synthesis gas to methanol. Although this process is industrially established, the costs of building and operating such a plant are high.[10] Alternatively, direct conversion of methane to methanol has been observed when a stepwise process is used over materials like copper or iron-exchanged zeolites;[11] however, such direct conversion is in its developmental infancy. The first Cu-exchanged zeolites to be reported to convert methane to methanol were Cu-ZSM-5 and MOR.[12,13] The initial yields were very low and the vast majority of the copper did not participate in the conversion. Over the course of the past 15 years, the methanol yield has steadily increased as each contribution to this field has improved our understanding of the extraction process,[14,15] cation exchange process,[16–18] and structure–property relationships.[19,30] However, numerous aspects of this process remain poorly understood and significant variation can be found in: methanol yields,[12–14,16,18,20,21] proposed active sites,[12,13,16,20,22–30] and observed differences in the oxidation and reduction of copper,[31] oftentimes even with the same zeolite framework and zeolite composition.

Zeolites are composed of silicon and aluminum atoms that are tetragonally coordinated (T-sites) to oxygens. These T-sites are arranged in a variety of ways that allow for over 232 zeolite structures.[32] They differ from each other in the pore size and the connectivity of each pore. Due to the different charges on the silicon and aluminum, when aluminum is

[a] *Institute for Chemical and Bioengineering, ETH Zurich, Vladimir-Prelog-Weg 1, 8093 Zurich, Switzerland. E-mail: jeroen.vanbokhoven@chem.ethz.ch*
[b] *Laboratory for Catalysis and Sustainable Chemistry, Paul Scherrer Institute, 5232 Villigen, Switzerland. E-mail: ana.pinar@psi.ch*

† Electronic supplementary information (ESI) available. See DOI: 10.1039/c9cy00013e

in the structure it produces a negative charge. This negative charge is balanced by a cation (*i.e.* copper or iron), and in a reaction such as methane to methanol conversion, this cation and associated oxygen form the active site. Zeolites are primarily made by hydrothermal synthesis, but for each zeolite there can be multiple different synthesis conditions; additionally, zeolites can go through post-synthetic treatment which adds further to the matrix of possible pathways to obtain a specific zeolite.[33] Across the methane to methanol literature, the source of the tested zeolite varies. Often times, zeolites such as mordenite and ZSM-5 are commercially purchased;[12–19,34–36] however, there is no overlap (or very rarely) in zeolite suppliers,[12,14,21,34] and the precise details of synthesis conditions or post-treatment are rarely publicly available. Meanwhile, other groups are synthesized in-house through hydrothermal synthesis.[20,37–39] It is well-known that subtleties in the synthesis process[33,40] can greatly affect various properties of the zeolite, including the morphology,[41] intergrowth,[42,43] and aluminum distribution.[44,45]

Mazzite (MAZ) rarely occurs naturally and has been reported to occur in two locations: Mont Semiol, Loire, France[46] and later in Boron, California, USA.[47] Mazzite was synthetically made through hydrothermal synthesis prior to its discovery in nature. The synthetic versions are referred to as omega zeolite[48] and ZSM-4.[49] However, currently, it isn't readily available commercially, and thus needs to be synthesized in-house. MAZ only has a narrow range of synthesis parameters,[50,51] and often is plagued by trace amounts of competing phases like sodalite, gismondine and MAZ's precursor, zeolite Y. Copper-exchanged MAZ with a sodalite co-phase has relatively high conversion of methane to methanol compared to other well-studied zeolites (*i.e.* mordenite),[52] and the methanol yield can be further increased by synthesizing pure MAZ.[53]

Through exploring simple changes in synthesis conditions of MAZ, we show that the methanol yield is greatly influenced by the morphology of the parent zeolite. Since most groups tackling the methane to methanol problem work on differently sourced zeolites, the wide range of methanol yields and observations may be at least partially explained by differences in the parent zeolite. More importantly, this fact makes it clear that the zeolite synthesis is one more opportunity for optimizing and ultimately improving the conversion of methane to methanol with zeolites.

Experimental

To study how minor changes in the synthesis could affect the methane to methanol conversion, omega zeolite (MAZ) was synthesized through the hydrothermal autogenous pressure synthesis technique. A gel slurry was prepared with a molar composition of $SiO_2 : Al_2O_3 : Na_2O : TMACl : water = 15.2 : 1 : 7.1 : 1.4 : 460$, and the molar composition was kept constant, but parameters like the rotation speed were altered. The slurry was placed into a 100 ml steel autoclave with a Teflon liner. For Cu-MAZ-fast and Cu-MAZ-slow, the only difference in the synthesis was that the slurries were subjected to two different rotational speeds during synthesis: 15 vertical turns per minute (Cu-MAZ-fast), and 5 vertical turns per minute (Cu-MAZ-slow).

Due to the narrow range of synthesis conditions, homogeneity is important for producing pure omega which is, in turn, promoted by rotating the autoclave during synthesis. The samples were kept in the oven at 378 K for 21 days. Both samples were calcined and ion exchanged in the same manner, and the details of the calcination and exchange procedures can be found in the ESI.† Both samples were then tested for the direct conversion of methane to methanol in two stepwise procedures: high temperature activation[12,14,16,34,52] under isobaric conditions, and high temperature activation with elevated methane pressure (6 bar).[27,54]

Results

The effect of the rotational speed during synthesis results in immense differences in the methanol yield for both procedures as shown in Fig. 1. For the conventional procedure, MAZ-slow yields nearly 1.5× more methanol than MAZ-fast with MAZ-slow producing 150.9 μmol per gram-zeolite, which is comparable with the highest values for mordenite.[55] With higher methane pressures, the methanol yield can be further increased for both samples. For MAZ-slow, the improvement of methanol yield by increasing the pressure is greater than that for MAZ-fast. With 6 bar methane, MAZ-slow can produce nearly twice that of MAZ-fast resulting in a yield for MAZ-slow of 197 μmol per gram-zeolite, the highest recorded yield thus far without the required higher methane pressures (30 bar) previously reported for Cu-MAZ.[53] This difference between MAZ-slow and MAZ-fast indicates that the conditions of the zeolite synthesis can significantly influence the performance of a material for the conversion of methane to methanol.

Despite the large differences in the performance in the conversion of methane to methanol, traditional characterization methods (*i.e.* BET, XRD, and NMR) show that both samples are very similar as shown in Fig. 2 and Table 1. The

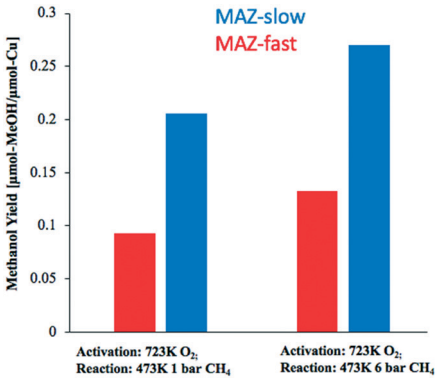

Fig. 1 Methanol yield per copper for MAZ-fast and MAZ-slow for different stepwise procedures for the conversion of methane to methanol. MAZ-slow outperforms MAZ-fast in both procedures.

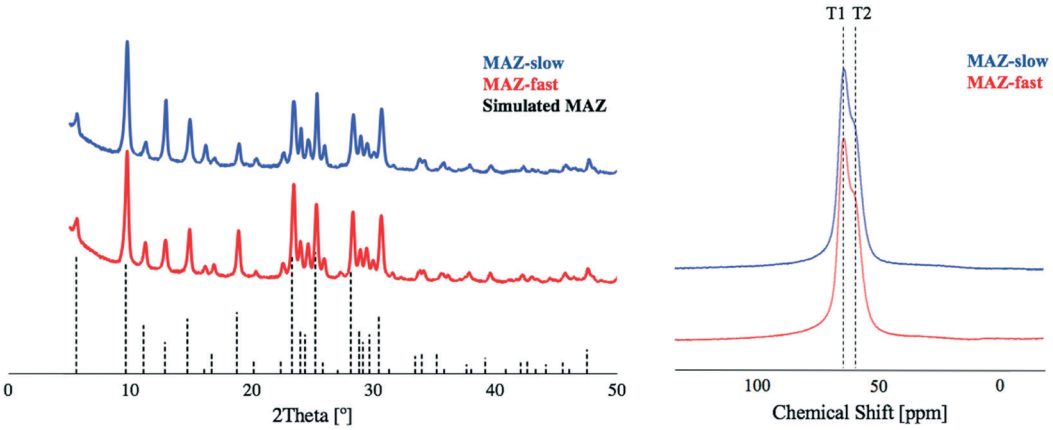

Fig. 2 (Left) XRD patterns of MAZ-fast and MAZ-slow after calcination at 550 °C. Both synthesis procedures produced pure MAZ. (Right) ^{27}Al MAS NMR spectrum of MAZ-slow and MAZ-fast after calcination at 550 °C. Cations were exchanged with ammonium for NMR analysis. No extra-framework aluminum is detected and the distributions in the two T-sites are similar.

Table 1 Summary of the synthesized MAZs at various stages (*i.e.* uncalcined, calcined and copper cation exchanged)

	Uncalcined		Calcined		Cation exchanged
Sample name	C/N ratio	Wt% organics	Si/Al	BET surface area (m^2 g^{-1})	Wt% Cu
MAZ-fast	3.77	5.64	4.32	137.0	4.78
MAZ-slow	3.75	5.40	4.25	135.9	4.64

hydrothermal synthesis of omega zeolite progresses very similarly for both samples with the aluminum and the structure directing agent (SDA) being incorporated into the zeolite with equivalent C/N and Si/Al ratios in Table 1. Fig. 2 shows that pure crystalline omega was formed in both cases with high crystallinity. Aluminum T-site occupancy is often alluded to as a reason for performance differences; however, the determination of aluminum distribution in T-sites is often an open question due to the difficulty in distinguishing silicon from aluminum in T-sites by XRD or indistinguishable sites by ^{27}Al NMR. Fortunately, in omega zeolite, there are two non-equivalent crystallographic T-sites, both of which are distinguishable in ^{27}Al MAS NMR spectra.[56] In Fig. 2 both samples yielded identical spectra and indicate no difference in aluminum distribution between T1 and T2 sites which therefore is not a reason for the observed differences in the performance.

To understand differences in the copper speciation, both samples were examined by FTIR spectroscopy and X-ray absorption spectroscopy (XAS). By using NO as a probe molecule with FTIR, the copper speciation for activated MAZ-fast and MAZ-slow was investigated. The resulting spectra in Fig. S5† show that a similar multiplicity of copper(II) sites is present in both materials. Additionally, *in situ* XAS at the Cu-K edge was used to probe the local electronic and geometric structure of copper during the activation and reaction at one or six bar methane. Fig. 3 shows that after activation, both XANES spectra are very similar in shape with a shoulder at 8986 eV which has been previously attributed to the dehydration of copper.[14] There is a slight difference in the maximum intensity with MAZ-fast showing a lower relative intensity and a small copper(I) shoulder at 8983 eV. A difference is also observed in the EXAFS spectra with a small enhancement in the intensity for the first shell (Cu–O) of MAZ-slow (Fig. S2†). This difference could be attributed to an increase of average local coordination to oxygen for MAZ-slow, and such a

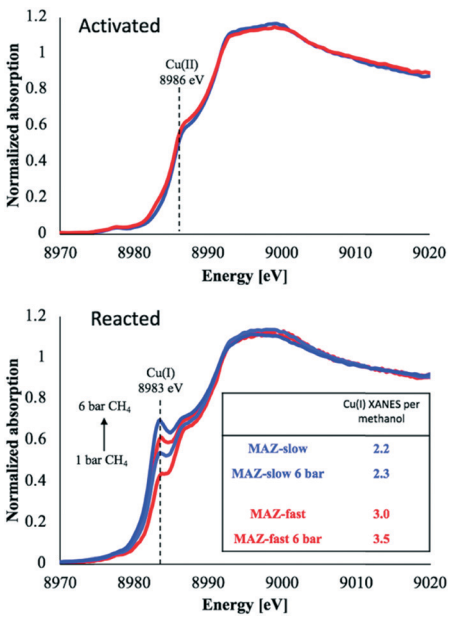

Fig. 3 (Top) Cu K-edge spectra of activated MAZ-slow and MAZ-fast. (bottom) Cu K-edge spectra of *in situ* stepwise conversion of MAZ-fast. Spectra were taken after reaction at one and six bar methane.

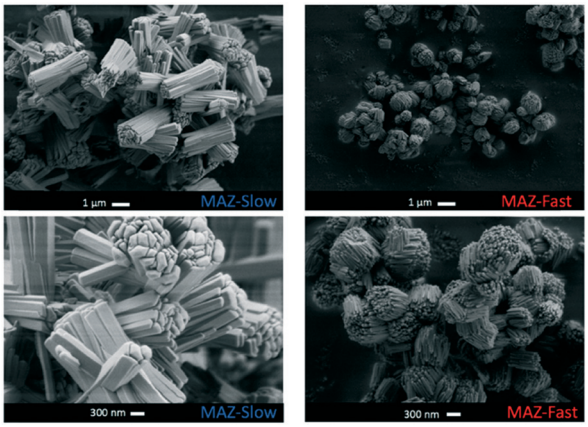

Fig. 4 SEM micrographs of MAZ-slow and MAZ-fast.

difference could be a result of differential diffusion of oxygen into the zeolites during activation. For the second shell, determination of speciation between Cu–O, Cu–Cu, and Cu–Al(Si) is inconclusive. The EXAFS spectra for both appear similar to previously reported spectra for activated MOR samples[16,26] with a copper nuclearity of one to three copper atoms as opposed to large copper agglomerates.

During interaction with methane, the conversion of copper(II) to copper(I) is greater for MAZ-slow with Cu(I) accounting for 44% of copper while for MAZ-fast the conversion to Cu(I) is less with only 26% as Cu(I) after reaction at 1 bar. As the methane pressure is increased, the copper(II) to copper(I) conversion increases further. Assuming a two-electron redox mechanism for the conversion of methane to methanol, MAZ-slow is near the expected two reduced coppers per methanol formed.[31] However for MAZ-fast, more copper(I) is formed per methanol yield. To further understand this difference, the reaction products were also examined by FTIR spectroscopy. Both samples were highly selective; however, there was relatively more carbon monoxide per methoxy species formed in MAZ-fast than MAZ-slow (Fig. S6†). Carbon monoxide requires reduction of six copper atoms during its formation and can contribute to the formation of Cu(I), though such a difference in selectivity does not fully explain the vast performance differences.

One observed difference between the two samples was the morphology and the crystallite size. The SEM micrographs in Fig. 4 show MAZ-slow having bundles of interconnected sticks with lengths of 2–4 μm and 100 nm thickness, and MAZ-fast having spherulitic aggregates of small rods with lengths of ~300 nm and 10 nm thickness.

Similar morphologies were also obtained by changing additional parameters of the synthesis (*i.e.* silicon source and structure directing agent). Morphology is not therefore purely dependent on the rotation. Long bundled rods were synthesized when Ludox SM-30 was used as the silicon source in both rotation regimes. Meanwhile, for the silicon source Ludox AS-30, small spherulitic particles were formed in both rotation regimes.

In all the cases, when the morphology was small spherulitic aggregates, the methanol yield was severely diminished as shown in Table 2. Conversely, in all the syntheses that produced long bundled rods, the methanol yields clustered around 140–150 μmol-methanol per gram zeolite showing that the morphology plays an important role in the resulting methanol yield.

Discussion

After the first patents of MAZ,[48] there was a spike in interest industrially and academically for its synthesis and performance in various catalytic reactions (*i.e.* hydrocracking and isomerization). The two morphologies that we observed in Fig. 4 have been observed previously under different synthesis conditions,[50,51,57,58] and these different syntheses and morphologies can lead to differences in thermal stability,[58] decomposition mechanism,[59] diffusion properties,[57] adsorption capabilities,[57] and coking susceptibility.[57] Ultimately, these subtle differences affect a zeolite's overall performance in different reactions. We observe that the methane to methanol reaction is no exception, and the synthesis and overall resulting morphology greatly affect the methanol yield.

The vast majority of syntheses lead to a similar morphology to that of MAZ-fast. Larger crystallites, specifically hexagonal shaped ones, were also reported and patented for their superior thermal stability relative to the smaller aggregates.[58]

Table 2 Additional synthesis for the formation of pure MAZ and the resulting morphologies. These additional MAZ samples were tested for the conversion of methane to methanol

Sample name	Cu (mg per g-zeolite)	Si/Al ratio	μmol-MeOH per g-zeo.	μmol-MeOH per μmol-Cu	Morphology
Varying the structure direction agent (TMABr and TMAOH)					
MAZ_TMABr	45.0	4.3	104	0.15	Small rod aggregates (500–800 nm)
MAZ_TMAOH	50.4	6.6	71.4	0.09	Spherulitic aggregates (200–300 nm)
Varying silicon source (slow rotation)					
MAZ_AS_slow[a]	48.2	4.1	98.3	0.13	Spherulitic aggregates (300–500 nm)
MAZ_SM_slow[b]	44.4	4.0	144.8	0.21	Long bundled rods (2–3 μm)
Varying silicon source (fast rotation)					
MAZ_SM_fast[b]	42.7	4.6	142.5	0.21	Long bundled rods (2–3 μm)
MAZ_AS_fast[a]	43.1	4.3	37.6	0.06	Spherulitic aggregates (300–400 nm)

[a] Silicon source Ludox AS-30. [b] Silicon source Ludox SM-30.

Morphologies with large crystallites can withstand temperatures as high as 1173 K, but the small spheroids start to decompose at 873 K.[58] Additional follow-up papers found the mechanism of decomposition and the crystallization between these two morphologies to be different as well.[59] However for the methane to methanol stepwise procedure, we are below such a temperature. Upon examination of the XRD pattern and aluminum NMR spectra after the reaction, there are no signs of degradation during the stepwise procedure (Fig. S1†).

Additionally, such MAZ morphologies have been studied for their differing diffusion and adsorption properties.[57] Diffusion limitations were generally observed across the tested catalytic reactions and led to deactivation and coking for reactions such as cracking of hydrocarbons.[51] The basic zeolite channel structure is responsible for its diffusion limitations. MAZ has unidirectional 12-membered channels (aperture: 7.5 Å) and 8-membered channels (aperture: 3.1 Å). The channels are separated by 4- and 5-membered rings which are too small for molecules to travel from the 12-membered channels to the 8-membered channels; therefore, the 12-membered channels and 8-membered channels operate independently from each other. The 8-membered channel is connected with the 8-membered ring of the gmelinite cage. In one diffusion study, omega zeolite's morphology affects greatly the diffusion coefficient.[57] Specifically, the larger particles like we observed for MAZ-slow have much higher diffusion rates than the small spherulitic aggregates which resemble the morphology of MAZ-fast.[57] Methane to methanol conversion is a stoichiometric rather than a catalytic process that requires the activation, reaction, and extraction to be performed as separate steps. The deleterious effects of specific morphologies like MAZ-fast can compound for each step of the methane to methanol procedure, resulting in unformed active sites, inaccessible active sites, and/or unextractable methanol and finally low methanol yields.

Conclusions

Synthesis-dependent properties are not unique to omega zeolite and have also been observed for other zeolites that are active in the conversion of methane to methanol. Our observation of more advantageous synthesis conditions and morphologies for the conversion of methane to methanol can be applied to other zeolites. The morphology is a direct result of how the crystals grow and can significantly affect various properties of the material, such as potential diffusion/adsorption limitations, pore blocking, and thermal stability.

Cu-MAZ has one of the highest reported methanol yields for the conversion of methane to methanol on copper-exchanged zeolites. Different synthesized morphologies result in differences in the methanol yield despite having similar Si/Al ratios, BET surface areas, aluminum T-site occupancies, copper speciation (FTIR and EXAFS), and XRD patterns. This highlights that the zeolite itself can greatly affect the success of methane to methanol conversion. For the methane to methanol community, this work shows that care should be taken when selecting a parent zeolite for such studies, but more importantly it highlights the opportunity that the zeolite itself has for optimizing this process.

Conflicts of interest

There are no conflicts to declare.

Acknowledgements

The authors would like to thank Dr. Hermann Emerich at the Swiss Norwegian beamline (BM 31) as well as Dipanjan Banerjee and Alessandro Longo at the Dutch Belgian beamline (BM26) at the ESRF. Dr. Pinar and Dr. Sushkevich acknowledge the Energy System integration (ESI) platform at the Paul Scherrer Institute for funding. Dr. Newton acknowledges Shell Global solutions for the funding of his position.

Notes and references

1 T. A. Brzustowski, *Prog. Energy Combust. Sci.*, 1976, **2**, 129.
2 M. R. Johnson and A. R. Coderre, *J. Air Waste Manage. Assoc.*, 2011, **61**, 190–200.
3 C. D. Elvidge, M. Zhizhin, K. Baugh, F. C. Hsu and T. Ghosh, *Energies*, 2016, **9**, 14.
4 J. H. Lunsford, *Catal. Today*, 2000, **63**, 165–174.
5 P. Tang, Q. Zhu, Z. Wu and D. Ma, *Energy Environ. Sci.*, 2014, **7**, 2580–2591.
6 N. R. Foster, *Appl. Catal.*, 1985, **19**, 1–11.
7 G. A. Olah, *Angew. Chem., Int. Ed.*, 2005, **44**, 2636–2639.
8 C. Hammond, S. Conrad and I. Hermans, *ChemSusChem*, 2012, **5**, 1668–1686.
9 A. Caballero and P. J. Pérez, *Chem. Soc. Rev.*, 2013, **42**, 8809.
10 J.-P. Lange, K. P. De Jong, J. Ansorge and P. J. A. Tijm, *Stud. Surf. Sci. Catal.*, 1997, **107**, 81–86.
11 B. E. R. Snyder, M. L. Bols, R. A. Schoonheydt, B. F. Sels and E. I. Solomon, *Chem. Rev.*, 2018, **118**, 2718–2768.
12 M. H. Groothaert, P. J. Smeets, B. F. Sels, P. A. Jacobs and R. A. Schoonheydt, *J. Am. Chem. Soc.*, 2005, **127**, 1394–1395.
13 P. J. Smeets, M. H. Groothaert and R. A. Schoonheydt, *Catal. Today*, 2005, **110**, 303–309.
14 E. M. Alayon, M. Nachtegaal, M. Ranocchiari and J. A. van Bokhoven, *Chem. Commun.*, 2012, **48**, 404–406.
15 N. V. Beznis, B. M. Weckhuysen and J. H. Bitter, *Catal. Lett.*, 2010, **138**, 14–22.
16 S. Grundner, M. A. C. Markovits, G. Li, M. Tromp, E. A. Pidko, E. J. M. Hensen, A. Jentys, M. Sanchez-Sanchez and J. A. Lercher, *Nat. Commun.*, 2015, **6**, 7546.
17 S. Grundner, W. Luo, M. Sanchez-Sanchez and J. A. Lercher, *Chem. Commun.*, 2016, **52**, 2553–2556.
18 H. V. Le, S. Parishan, A. Sagaltchik, C. Göbel, C. Schlesiger, W. Malzer, A. Trunschke, R. Schomäcker and A. Thomas, *ACS Catal.*, 2017, **7**, 1403–1412.
19 P. Vanelderen, B. E. R. Snyder, M. L. Tsai, R. G. Hadt, J. Vancauwenbergh, O. Coussens, R. A. Schoonheydt, B. F. Sels and E. I. Solomon, *J. Am. Chem. Soc.*, 2015, **137**, 6383–6392.

20 D. K. Pappas, E. Borfecchia, M. Dyballa, I. A. Pankin, K. A. Lomachenko, A. Martini, M. Signorile, S. Teketel, B. Arstad, G. Berlier, C. Lamberti, S. Bordiga, U. Olsbye, K. P. Lillerud, S. Svelle and P. Beato, *J. Am. Chem. Soc.*, 2017, **139**, 14961.
21 V. L. Sushkevich and J. van Bokhoven, *Catal. Sci. Technol.*, 2018, **8**, 4141–4150.
22 J. S. Woertink, P. J. Smeets, M. H. Groothaert, M. A. Vance, B. F. Sels, R. A. Schoonheydt and E. I. Solomon, *Proc. Natl. Acad. Sci. U. S. A.*, 2009, **106**, 18908–18913.
23 P. J. Smeets, R. G. Hadt, J. S. Woertink, P. Vanelderen, R. A. Schoonheydt, B. F. Sels and E. I. Solomon, *J. Am. Chem. Soc.*, 2010, **132**, 14736–14738.
24 P. Vanelderen, J. Vancauwenbergh, B. F. Sels and R. A. Schoonheydt, *Coord. Chem. Rev.*, 2013, **257**, 483–494.
25 P. Vanelderen, B. E. R. Snyder, M. L. Tsai, R. G. Hadt, J. Vancauwenbergh, O. Coussens, R. A. Schoonheydt, B. F. Sels and E. I. Solomon, *J. Am. Chem. Soc.*, 2015, **137**, 6383–6392.
26 E. M. C. Alayon, M. Nachtegaal, A. Bodi, M. Ranocchiari and J. A. van Bokhoven, *Phys. Chem. Chem. Phys.*, 2015, **17**, 7681.
27 P. Tomkins, A. Mansouri, S. E. Bozbag, F. Krumeich, M. B. Park, E. M. C. Alayon, M. Ranocchiari and J. A. van Bokhoven, *Angew. Chem., Int. Ed.*, 2016, **55**, 5557–5561.
28 D. Palagin, A. J. Knorpp, A. B. Pinar, M. Ranocchiari and J. A. van Bokhoven, *Nanoscale*, 2017, **9**, 1144–1153.
29 A. R. Kulkarni, Z. Zhao, S. Siahrostami, J. K. Nørskov and F. Studt, *Catal. Sci. Technol.*, 2017, **8**, 114–123.
30 E. Borfecchia, D. K. Pappas, M. Dyballa, K. A. Lomachenko, C. Negri, M. Signorile and G. Berlier, *Catal. Today*, 2018, 0–11.
31 M. A. Newton, A. J. Knorpp, A. B. Pinar, V. L. Sushkevich, D. Palagin and J. A. Van Bokhoven, *J. Am. Chem. Soc.*, 2018, **140**, 10090–10093.
32 C. Baerlocher and L. B. McCusker, *Database of Zeolite Structures*, http://www.iza-structure.org/databases/.
33 J. Cejka, H. V. Bekkum, A. Corma and F. Schueth, in *Introduction to Zeolite Science and Practice*, Elsevier Science, Amsterdam, 3rd edn, 2007.
34 P. Vanelderen, J. Vancauwenbergh, M. L. Tsai, R. G. Hadt, E. I. Solomon, R. A. Schoonheydt and B. F. Sels, *ChemPhysChem*, 2014, **15**, 91–99.
35 M. A. C. Markovits, A. Jentys, M. Tromp, M. Sanchez-Sanchez and J. A. Lercher, *Top. Catal.*, 2016, **59**, 1554–1563.
36 A. J. Knorpp, M. A. Newton, A. B. Pinar and J. A. van Bokhoven, *Ind. Eng. Chem. Res.*, 2018, **57**, 12036–12039.
37 M. J. Wulfers, S. Teketel, B. Ipek and R. F. Lobo, *Chem. Commun.*, 2015, **51**, 4447–4450.
38 C. Paolucci, A. A. Parekh, I. Khurana, J. R. Di Iorio, H. Li, J. D. Albarracin Caballero, A. J. Shih, T. Anggara, W. N. Delgass, J. T. Miller, F. H. Ribeiro, R. Gounder and W. F. Schneider, *J. Am. Chem. Soc.*, 2016, **138**, 6028–6048.
39 K. Narsimhan, K. Iyoki, K. Dinh and Y. Román-Leshkov, *ACS Cent. Sci.*, 2016, **2**, 424–429.
40 M. Moliner, C. Martínez and A. Corma, *Angew. Chem., Int. Ed.*, 2015, **54**, 3560–3579.
41 Y. Mao, Y. Zhou, H. Wen, J. Xie, W. Zhang and J. Wang, *New J. Chem.*, 2014, **38**, 3295–3301.
42 J. D. Sherman and J. M. Bennett, in *Advances in Chemistry*, ed. W. M. Meier and J. B. Uytterhoeven, 1973, pp. 52–65.
43 D. G. Hay, H. Jaeger and K. G. Wilshier, *Zeolites*, 1990, **10**, 571.
44 V. Gábová, J. Dědeček and J. čejka, *Chem. Commun.*, 2003, 1196–1197.
45 J. R. Di Iorio and R. Gounder, *Chem. Mater.*, 2016, **28**, 2236.
46 E. Galli, E. Passaglia, D. Pongiluppi and R. Rinaldi, *Contrib. Mineral. Petrol.*, 1974, **45**, 99–105.
47 R. Arletti, E. Galli, G. Vezzalini and W. S. Wise, *Am. Mineral.*, 2005, **90**, 1186–1191.
48 Union Carbide Corporation, *NL Pat.*, 6710729, 1968.
49 Mobil Oil Corporation, *GB Pat.*, 1117568, 1968.
50 F. Fajula, M. Vera-Pacheco and F. Figueras, *Zeolites*, 1987, **7**, 203–208.
51 A. J. Perrotta, C. Kibby, B. R. Mitchell and E. R. Tucci, *J. Catal.*, 1978, **55**, 240–249.
52 M. B. Park, S. H. Ahn, A. Mansouri, M. Ranocchiari and J. A. van Bokhoven, *ChemCatChem*, 2017, **9**, 3705–3713.
53 A. J. Knorpp, A. B. Pinar, M. Newton, V. Sushkevich and J. A. van Bokhoven, *ChemCatChem*, 2018, 1–5.
54 P. Tomkins, M. Ranocchiari and J. A. van Bokhoven, *Acc. Chem. Res.*, 2017, **50**, 418–425.
55 D. K. Pappas, A. Martini, M. Dyballa, K. Kvande, S. Teketel, K. A. Lomachenko, R. Baran, P. Glatzel, B. Arstad, G. Berlier, C. Lamberti, S. Bordiga, U. Olsbye, S. Svelle, P. Beato and E. Borfecchia, *J. Am. Chem. Soc.*, 2018, **140**, 15270–15278.
56 P. Massiani, F. Fajula, F. Figueras and J. Sanz, *Zeolites*, 1988, **8**, 332–337.
57 B. Chauvin, F. Fajula, F. Figueras, C. Gueguen and J. Bousquet, *J. Catal.*, 1988, **111**, 94–105.
58 F. Fajula, F. Figueras, L. Moudafi, V. M. Pacheco, S. Nicolas, P. Dufresne and C. Gueguen, *US Pat.*, 4891200, 1990.
59 A. Maubert, R. Dutartre, L. C. de Menorval and F. Figueras, *Zeolites*, 1993, **13**, 587–591.